The Planetary Science Journal, 2:68 (12pp), 2021 April https://doi.org/10.3847/PSJ/abe76f

The Role of Hydrated Minerals and Space Weathering Products in the Bluing of Carbonaceous Asteroids

David Trang[1], Michelle S. Thompson[2], Beth E. Clark[3], Hannah H. Kaplan[4], Xiao-Duan Zou[5], Jian-Yang Li[5], Salvatore M. Ferrone[3], Victoria E. Hamilton[6], Amy A. Simon[4], Dennis C. Reuter[4], Lindsay P. Keller[7], M. Antonietta Barucci[8], Humberto Campins[9], Cateline Lantz[10], Daniella N. DellaGiustina[11], Ronald-Louis Ballouz[11], Erica R. Jawin[12], Harold C. Connolly, Jr.[11,13], Kevin J. Walsh[6], and Dante S. Lauretta[11]
[1] Hawai'i Institute of Geophysics and Planetology, University of Hawai'i at Mānoa, Honolulu, HI, USA; dtrang@higp.hawaii.edu
[2] Department of Earth, Atmospheric, and Planetary Sciences, Purdue University, West Layfette, IN, USA
[3] Department of Physics and Astronomy, Ithaca College, Ithaca, NY, USA
[4] NASA Goddard Space Flight Laboratory, Greenbelt, MD, USA
[5] Planetary Science Institute, Tucson, AZ, USA
[6] Southwest Research Institute, Boulder, CO, USA
[7] NASA Johnson Space Center, Houston, TX, USA
[8] LESIA, Observatoire de Paris, Université PSL, CNRS, Université de Paris, Sorbonne Université, France, Paris, France
[9] Department of Physics, University of Central Florida, Orlando, FL, USA
[10] Institut d'Astrophysique Spatiale, CNRS/Université Paris-Saclay, Orsay, France
[11] Lunar and Planetary Laboratory, University of Arizona, Tucson, AZ, USA
[12] Smithsonian Institution, Washington DC, USA
[13] School of Earth and Environment, Rowan University, Glassboro, NJ, USA
Received 2020 November 24; revised 2021 February 8; accepted 2021 February 16; published 2021 April 6

Abstract

The surfaces of airless bodies such as lunar and S-type asteroids typically become spectrally redder in visible to near-infrared reflectance with longer exposures to space weathering. However, some carbonaceous asteroids instead become spectrally bluer. Space weathering experiments on carbonaceous meteorites have provided some clues as to the space weathering products that could produce spectral bluing. We applied these experimental results to our Hapke radiative transfer model, with which we modeled spectral data from the OSIRIS-REx mission in order to determine whether these space weathering products—specifically, nanophase and microphase metallic iron, troilite, and magnetite—could explain the globally blue spectrum of the carbonaceous asteroid (101955) Bennu. The model suggests that the surface of Bennu has microphase iron, nanophase magnetite, and nanophase and microphase troilite. Considering previous space weathering experiments together with our spectral modeling of Bennu, we posit that the presence of nanophase magnetite is what causes a carbonaceous asteroid to become spectrally bluer with exposure time. Nanophase magnetite can form on asteroids that have Fe-bearing hydrated minerals (phyllosilicates). On anhydrous carbonaceous asteroids, nanophase iron forms instead of magnetite, leading to spectral reddening. We therefore predict that samples returned by the OSIRIS-REx mission from Bennu will have more nanophase magnetite than nanophase iron with nanophase and microphase sulfides, whereas samples returned by the Hayabusa2 mission from the carbonaceous asteroid (162173) Ryugu, which is spectrally red, will contain nanophase and microphase sulfides as well as more nanophase iron than nanophase magnetite.

Unified Astronomy Thesaurus concepts: Near-Earth objects (1092); Planetary surfaces (2113); Spectroscopy (1558)

1. Introduction

Studies of airless bodies such as the Moon and S-type asteroids have shown that with long durations of exposure to micrometeoroid bombardment and solar wind—processes collectively known as space weathering—the visible to near-infrared reflectance spectra of an exposed surface becomes spectrally redder (increasing reflectance with increasing wavelength) (e.g., Keller & McKay 1993, 1997; Hapke 2001; Noguchi et al. 2011). Exposure to space weathering causes surface material to experience physical and chemical changes. One such outcome of space weathering is the development of submicroscopic particles. Owing to their small size, these particles can cause a reflectance spectrum to redden by Rayleigh scattering (Hapke 2001).

Our current understanding and models of space weathering on airless bodies (e.g., Cassidy & Hapke 1975; Hapke 2001; Noble et al. 2007; Lucey & Riner 2011) have largely been shaped by knowledge gained from investigations of lunar regolith. These lunar space weathering studies showed that the presence of submicroscopic particles affects the overall reflectance slope in the visible to near-infrared (Cassidy & Hapke 1975; Keller & McKay 1993, 1997). Within the lunar regolith, submicroscopic particles reside inside agglutinates (aggregates of mineral fragments welded by impact glass) and glassy patinas around micron-sized mineral grains. These submicroscopic particles can be subdivided on the basis of size into nanophase (<40 nm) and microphase (>40 nm) particles (Noble et al. 2007). Because the main minerals on the lunar surface are plagioclase, pyroxene, and olivine, the submicroscopic particles predominantly consist of metallic iron (Fe).

The presence of nanophase iron particles in a regolith causes a spectrum to darken and redden, whereas the presence of microphase iron particles causes a spectrum to only darken. However, asteroids have a different and more complex mineralogy than the Moon, which could mean that space weathering may produce submicroscopic particles that contain opaque minerals other than iron. For instance, samples returned from asteroid Itokawa exhibit not only iron nanoparticles, but submicroscopic sulfide particles as well (Noguchi et al. 2011, 2014).

Spectral reddening is not universally observed for carbonaceous asteroids, which are primitive rocky bodies that are characterized by their low albedo and relatively high abundance of carbon. Although some carbonaceous asteroids are spectrally red, as expected with exposure to space weathering, others are spectrally blue in the visible to near-infrared wavelengths (decreasing reflectance with increasing wavelength) (e.g., Nesvorný et al. 2005). Spectral bluing of asteroid surfaces cannot be explained by lunar-like space weathering.

Previous work has attempted to address this conundrum by examining spectral characteristics of asteroid populations (Nesvorný et al. 2005; Lazzarin et al. 2006) and simulating space weathering of meteorites (e.g., Moroz et al. 2004b; Matsuoka et al. 2015; Gillis-Davis et al. 2017; Lantz et al. 2017; Thompson et al. 2019; Hiroi et al. 2020) and analog terrestrial material in the laboratory (e.g., Rubino et al. 2020). Space weathering experiments have revealed conflicting spectral trends dependent on the analog carbonaceous meteorite type (full descriptions of these types can be found in Scott & Krot (2007) and Krot et al. (2014)) and the simulated space weathering process employed. Though detailed optical characterizations were performed, not all experimental space weathering studies focused on determining the microstructural or chemical space weathering product responsible for the resultant spectral properties.

Space weathering laboratory experiments mimic one of the two main space weathering processes—micrometeoroid or solar wind bombardment—at a time, through laser and ion irradiation, respectively. Experimental space weathering of carbonaceous chondrites, which are suggested to originate from carbonaceous asteroids, has not resulted in the same spectral and compositional changes as the natural and experimental weathering of lunar material (e.g., Nesvorný et al. 2005; Lazzarin et al. 2006; Moroz et al. 2004b; Gillis-Davis et al. 2017; Lantz et al. 2017; Thompson et al. 2020) (see Table 1). For example, simulated micrometeoroid bombardment experiments on CV and CM chondrites consistently produced submicroscopic sulfides, e.g., troilite and pentlandite (Gillis-Davis et al. 2017; Thompson et al. 2019, 2020). These sulfides ranged in size from 5 to 3000 nm and occurred both in vapor deposits and on surfaces of the host grains as splash melts, which suggests the presence of sulfides in both nanophase and microphase forms. Laser irradiation experiments on a CM meteorite resulted in nanophase magnetite particles in the vapor deposit on the surfaces of the host grains. Simulated micrometeoroid bombardment on CM (Murchison and Mighei), CI (Orgueil and Ivuna), and C2-ungrouped (Tagish Lake) chondrites resulted in darkening and bluing (Hiroi et al. 2013; Matsuoka et al. 2015; Thompson et al. 2020). Conversely, laser irradiation of CV, CO, and CK meteorites generally resulted in darkening and reddening (Hiroi et al. 2013; Gillis-Davis et al. 2017).

As shown in Table 1, simulated solar wind experiments on carbonaceous chondrites have produced inconsistent results, including bluing and brightening (Vernazza et al. 2013; Lantz et al. 2017; Laczniak et al. 2020), reddening and darkening (Keller et al. 2015), and no change (Lantz et al. 2015). The reddening and darkening observed by Keller et al. (2015) in a CM chondrite was attributed to the development of nanophase iron and sulfides (Keller et al. 2015), whereas the bluing and brightening observed in other experiments on CM chondrites has been suggested to be due to carbonization, where in this context, the hydrocarbon experiences hydrogen loss and the aromatic carbon structures become larger (Moroz et al. 2004b; Lantz et al. 2017).

In our study, we address the conundrum of spectral bluing versus reddening in carbonaceous asteroids by using a physics-based space weathering spectral model that is constrained by the published results of space weathering experiments. We model the visible to near-infrared spectra of the hydrated spectrally blue carbonaceous asteroid (101955) Bennu (Clark et al. 2011; Hamilton et al. 2019; Simon et al. 2020) as observed by the OSIRIS-REx Visible to Near-InfraRed Spectrometer (OVIRS; Reuter et al. 2018). We use these results to explore which space weathering product is likely the cause of the spectral bluing that occurs on some carbonaceous asteroids and whether the space weathering products observed in the laboratory can also exist on these asteroids.

2. Methods

The physics-based Hapke radiative transfer model has been used to map the submicroscopic particle abundances on both Mercury (Trang et al. 2017) and the Moon (Trang & Lucey 2019). Further, Trang & Lucey (2019) showed that, based upon lunar samples, this model can predict the abundance of the space weathering products' nanophase and microphase iron to 0.1 and 0.6 wt% Fe, respectively, assuming that the physical and mineralogical parameters of the regolith are known. In this study, we used the Hapke radiative transfer technique: (1) to determine how the presence of submicroscopic particles produced by space weathering in regolith affects visible to near-infrared reflectance (i.e., which of these particles are likely to cause spectral bluing or reddening), and (2) to determine whether these submicroscopic particles could explain the spectrally blue surface of Bennu, as observed by OVIRS.

2.1. Modeling the Spectral Effects of Various Submicroscopic Particles

In our initial phase of modeling, we focused on nanophase and microphase iron, troilite, and magnetite, because these have been observed to form as products in space weathering experiments on carbonaceous chondrites (e.g., Thompson et al. 2020), suggesting that they may also form on the surfaces of carbonaceous asteroids. To model the spectral effects of these species, we made several assumptions about their physical and compositional characteristics, as well as those of their host particles.

Specifically, we assumed a regolith consisting of 15 μm diameter quartz particles. We selected quartz as a host because it is spectrally neutral and bright, and thus will easily show the spectral effects of the submicroscopic particles, whereas other

Table 1
Spectral and Compositional Summary of Space Weathering Experiment Results on Various Carbonaceous Meteorites

			Spectral Response		TEM Study						
	Micrometeoroid Impact Experiments	Type	Slope	Overall	npFe	mpFe	npMag	mpMag	npTro	mpTro	Notes
Hydrous	Moroz et al. (2004a)	CM	Red	Darker							Irradiated mostly olivine
	Matsuoka et al. (2015)	CM	Blue	Darker							FeS-rich amorphous silicate detected
	Matsuoka et al. (2020)	CM	Blue	Darker							FeS-rich amorphous silicate detected
	Thompson et al. (2020)	CM	Blue	Darker	X		X		X	X	Became brighter after initial irradiation
	Hiroi et al. (2013)	CM	Blue	Darker							
	Hiroi et al. (2013)	CI	Blue	Darker							
	Hiroi et al. (2013)	Tagish Lake	Blue	Darker							
Anhydrous	Gillis-Davis et al. (2017)	CV	Red	Darker	X	X			X		
	Hiroi et al. (2013)	CO	Red	Darker							
	Hiroi et al. (2013)	CK	Red	Darker							
	Hiroi et al. (2013)	Howardite	Red	Darker							
	Solar Wind Experiments										
Hydrous	Lantz et al. (2017)	CM	Blue	Brighter							
	Lantz et al. (2015)	CM	No change	No Change							
	Keller et al. (2015)	CM	Red	Darker	X				X	X	
	Lantz et al. (2017)	CI	Blue	Brighter							
	Lantz et al. (2017)	Tagish Lake	Blue	Brighter							
	Vernazza et al. (2013)	Tagish Lake	Blue	Brighter							
Anhydrous	Lantz et al. (2017)	CV	Red	Darker							
	Brunetto et al. (2014)	CV	Red	Darker							
	Lazzarin et al. (2006)	CV	Red	Darker							
	Lantz et al. (2017)	CO	Red	Darker							
	Lazzarin et al. (2006)	CO	Red	Darker							

Notes. Here, np is the abbreviation used for nanophase, mp is microphase, Mag is magnetite, and Tro is troilite; npTro and mpTro can also indicate pentlandite.

minerals with a red or blue continuum slope (e.g., olivine, pyroxene, plagioclase) would make it harder to disentangle the effects of the submicroscopic particles. For the optical properties of quartz, we used the optical constants from a refractive index database (www.refractiveindex.info) where the constants were measured similarly to the work of Gao et al. (2012). To model the single-particle phase function (the average of the angular scattering function of particles with various sizes, shapes, and mineralogy; see Hapke (2012)), we used the values found in Lucey (1998), which represent average values of silicates (Mustard & Pieters 1989) (Table 2).

We treated nanophase particles as Rayleigh scatterers, as modeled by Hapke (2001), and microphase particles as Mie scatterers, based on the model of Lucey & Riner (2011). We applied the optical constants of Cahill et al. (2012) to model iron, those of Egan & Hilgeman (1977) to model troilite, and Querry (1985) to model magnetite. We assumed a size of 1 μm for the microphase particles and <40 nm for the nanophase particles.

With these assumptions, we modeled the quartz host with 0.1 wt.% of each particle type (i.e., nanophase and microphase iron, troilite, and magnetite) at a time, for a total of six different model reflectance spectra (Figure 1).

2.2. Modeling OVIRS Data

After characterizing the spectral effects of these six submicroscopic space weathering products, we determined which are needed to reproduce the OVIRS spectra. The OVIRS instrument is a point spectrometer that covers the visible to near-infrared wavelengths (Reuter et al. 2018). The spectrometer has a spectral range of 0.4–4.3 μm with a spectral resolution of 2–5 nm. For this study, we used global, spatially resolved OVIRS data (Reuter et al. 2019) from observations within $\sim 8^\circ$ phase angle. These observations came from the Detailed Survey phase of the OSIRIS-REx mission, specifically the 12:30 pm (local solar time) Equatorial Station (Lauretta et al. 2017, 2021; Simon et al. 2020). We filtered out data with emission angles $>70^\circ$ associated with high latitudes and limbs, as this is the threshold for the best-quality data (Zou et al. 2021). The sampling area on the surface for each spectrum (i.e., the footprint) is $\sim$20 m.

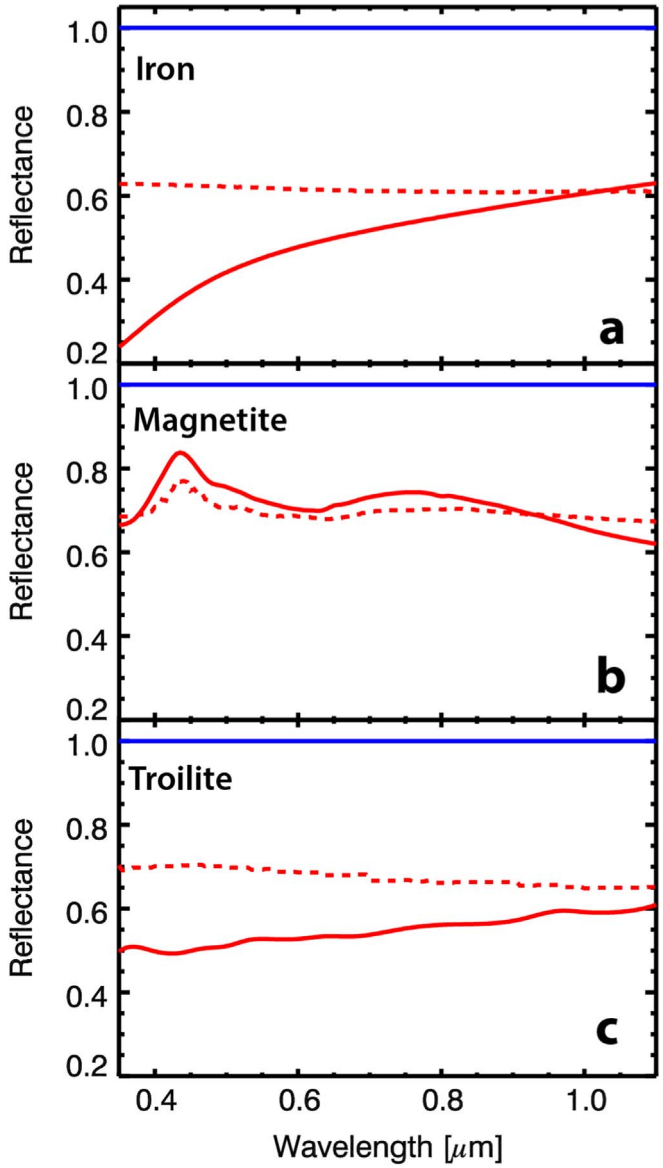

Figure 1. Spectral models of quartz (black line) and quartz with 0.01 wt% (a) iron, (b) magnetite, and (c) troilite. Microphase particles are shown as dashed red lines, nanophase as solid red lines.

To model this data set with the radiative transfer technique, a photometric correction is necessary. The photometric modeling and correction of OVIRS data are described by Zou et al. (2021). The photometric correction included converting the observed geometry of the OVIRS data to the common laboratory geometry (i_0, e_0, α_0) = (30°, 0°, 30°), where i_0, e_0, and α_0 are incidence, emission, and phase angle, respectively. Because of the limitations imposed by our spectral resolution and the range of our optical constants being lower than those of the OVIRS data, we did not use the entire OVIRS spectral range and resolution; our range was limited to 0.4–1.2 μm with a spectral resolution of 30–40 nm.

Although the surface of Bennu is dominantly covered with boulders (DellaGiustina et al. 2019), our model assumes that the surface has a regolith consisting of fine-particulate material; thus, it is likely modeling the fine dust that may be present on Bennu's surface (Hamilton et al. 2021, in revision) and mimicking the surface roughness of the boulders (further explored in Section 4.4). We assumed that our modeled fine-particulate material, i.e., the host particles, consist of a generic silicate (not quartz as in the last section) with a very low reflectance and a mineral density of 3.0 g cm^{-3} (the approximate average density of silicate minerals). We used silicates because our model relies on transparent minerals and cannot input submicroscopic particles in opaques. We also assumed that the regolith has a uniform particle size of 45 μm. In addition, this particle size, which influences the overall reflectance, resulted in reasonable submicroscopic particle abundances that are within the range of those found on the Moon (Trang & Lucey 2019). Because we are assuming silicates, we used a single-particle phase function in the form of a two-term Legendre polynomial with the same constants for b and c as Lucey (1998) (see Table 2). We also assumed that the real index of refraction (n) of the host is 1.5 throughout the visible and near-infrared, and that the imaginary index of refraction is a product of 0.002 times the wavelength of light (λ) in microns. This results in the host particles having a constant reflectance of 3.3% throughout the visible and near-infrared (Section 4.4). Together with the grain size, this assumption of the host reflectance results in reasonable submicroscopic particle abundances.

Table 2
Assumptions for the Various Model Parameters

Parameter	Value
i_0	30°
e_0	0°
α_0	30°
Host grain size	45 μm
Host reflectance	3.30%
Host particle density	3 g cm^{-3}
Host b	−0.4
Host c	0.25
Host n	1.5
Host k	0.002λ
Microphase size	1 μm

In our model, the nanophase particles were on the rims of the silicates and microphase particles were within the silicates, as observed in lunar regolith (e.g., Keller & Clemett 2001). We assume that each nanophase and microphase particle consists either of iron, magnetite, or troilite, based upon experiments on CM chondrites (Thompson et al. 2019, 2020), the meteorites most similar to Bennu (e.g., Clark et al. 2011; Hamilton et al. 2019). The assumed optical and physical properties of the submicroscopic particles were the same as in our test of their spectral effects (Section 2.1).

We calculated the absorption coefficients, given the above assumptions and using equations from Hapke (2001) and Lucey & Riner (2011), to determine the modeled single scattering albedo spectrum. With knowledge of the incidence and emission angles of the photometrically corrected OVIRS data, we converted the modeled single scattering albedo to reflectance to produce a modeled reflectance spectrum (Lucey 1998; Lucey & Riner 2011).

With this approach, we are able to build a model reflectance spectrum for any abundance of nanophase and microphase iron, magnetite, and troilite. We produced thousands of model spectra with different combinations of submicroscopic particle abundances; these model spectra make up our spectral library (Table 3). The upper limit for the abundance of nanophase and

Table 3
Summary of Minimum and Maximum Abundances of Submicroscopic Particles Included in the Spectral Library, and the Increments between the Abundances

	Increments [wt%]	Minimum [wt%]	Maximum [wt%]
Nanophase Iron	0.1	0	0.9
Microphase Iron	0.1	0	1.4
Nanophase Magnetite	0.1	0	1.5
Microphase Magnetite	0.1	0	1.5
Nanophase Troilite	0.1	0	1.5
Microphase Troilite	0.1	0	1.5

microphase particles was bounded based on the saturation limits as observed in lunar materials (Trang & Lucey 2019). We compared each OVIRS spectrum to model reflectance spectra that had a 750 nm reflectance that was within 0.1% of the 750 nm absolute reflectance in the OVIRS spectrum and obtained a root mean square (rms). Because we knew the submicroscopic particle abundances associated with each model spectrum, we were able to infer the submicroscopic particle abundance for each OVIRS spectrum from the best-matching (lowest rms) model spectrum.

We then produced maps of modeled submicroscopic particle abundances on Bennu by taking the modeled abundances for each OVIRS footprints and combining them onto a faceted shape model of Bennu constructed from lidar-based OSIRIS-REx Laser Altimeter (OLA) data (v20) (Barnouin et al. 2020; http://sbmt.jhuapl.edu/). We used a shape model with 49,152 facets to make spectral maps that are registered to the irregular shape of the asteroid. At each facet, the values from multiple overlapping OVIRS footprints were averaged, with each value weighted by its error in the average calculation. Uncertainties for each footprint value were similarly combined on the facets, to produce a one-sigma standard error map. This method takes the ~20 m OVIRS spots and places them on the shape model with a resolution of ~6 m per facet side.

3. Results

3.1. Spectral Effects of Different Submicroscopic Particles in a Neutral Host

The results of our modeling of the submicroscopic particles in the quartz host indicate that the presence of nanophase iron leads to darkening and reddening, whereas microphase iron causes the spectrum to only darken, as expected (Noble et al. 2007) (Figure 1(a); Table 4). Similarly, the presence of nanophase troilite causes darkening and reddening, but microphase troilite leads to darkening and a slight bluing (Figure 1(c); Table 3). Nanophase and microphase magnetite both cause an overall bluing with a local spectral maximum at 0.45 μm and another, broader local spectral maximum at about 0.75 μm (Figure 1(b); Table 3). Thus, the models indicate that microphase troilite and nanophase and microphase magnetite are the only particles out of those tested that could cause the spectral bluing in the visible to near-infrared spectra of carbonaceous asteroids such as Bennu.

3.2. Maps of Submicroscopic Space Weathering Products on Bennu's Surface

Using the OVIRS data, our model consistently mimics the blue-sloped spectrum of Bennu (Figures 2(a), (b)). Maps produced from the model output for each studied submicroscopic particle exhibit different distributions and abundances

Table 4
Visible to Near-infrared Spectral Characteristics of Submicroscopic Particles Embedded in a Quartz Host

	Spectral Slope	Unique Spectral Features
Nanophase Iron	Red	Bend at 0.5 μm
Microphase Iron	Flat	None
Nanophase Magnetite	Blue	Reflectance peak at 0.45 and 0.75 μm
Microphase Magnetite	Blue	Reflectance peak at 0.45 μm
Nanophase Troilite	Red	None
Microphase Troilite	Flat–Blue	None

(Figure 3). Because our model has not been calibrated to samples returned from Bennu, the mapped abundances are relative values in this study; to obtain absolute values, our model requires calibration using TEM, SEM, and magnetic analyses of the return samples.

Nanophase iron and microphase magnetite appear to be absent or negligible on the surface, with average abundances and standard deviations of 0.0 ± 0.0 wt% for both particle types (see panels (a) and (d), respectively, of Figure 3). In contrast, the models indicate intermediate average abundances of nanophase troilite (0.1 ± 0.0 wt%) (Figure 3(e)), microphase iron (0.2 ± 0.1 wt%) (Figure 3(b)), and nanophase magnetite (0.2 ± 0.0 wt%) (Figure 3(c)), and comparatively high average abundances of microphase troilite (1.0 ± 0.1 wt%) (Figure 3(f)).

The space weathering maps indicate a spatial correlation with albedo and areas containing large boulders (see Bennett et al. 2020; DellaGiustina et al. 2020). For example, a large region containing high abundances of nanophase and microphase troilite appears to overlap with Tlanuwa Regio, an area on Bennu's surface that contains a high density of large, dark boulders (Figure 3(e)–(f)). Nanophase magnetite appears to have a similar spatial correlation (Figure 3(c)). This same correspondence is also seen with two individual large dark boulders, Roc and Huginn (Figure 3(c), (e)–(f)). We also observe a region that contains some of the highest nanophase iron abundances (Figure 3(a)) but also some of the lowest nanophase troilite abundance (Figure 3(e)) in the southern hemisphere, which is associated with one of the largest dark boulders on Bennu, Benben.

4. Discussion

4.1. Modeled Abundances versus Laboratory Results

Our modeling of the OVIRS data suggests that Bennu's surface contains very low abundances of nanophase iron, but somewhat greater abundances of microphase iron (Figure 3).

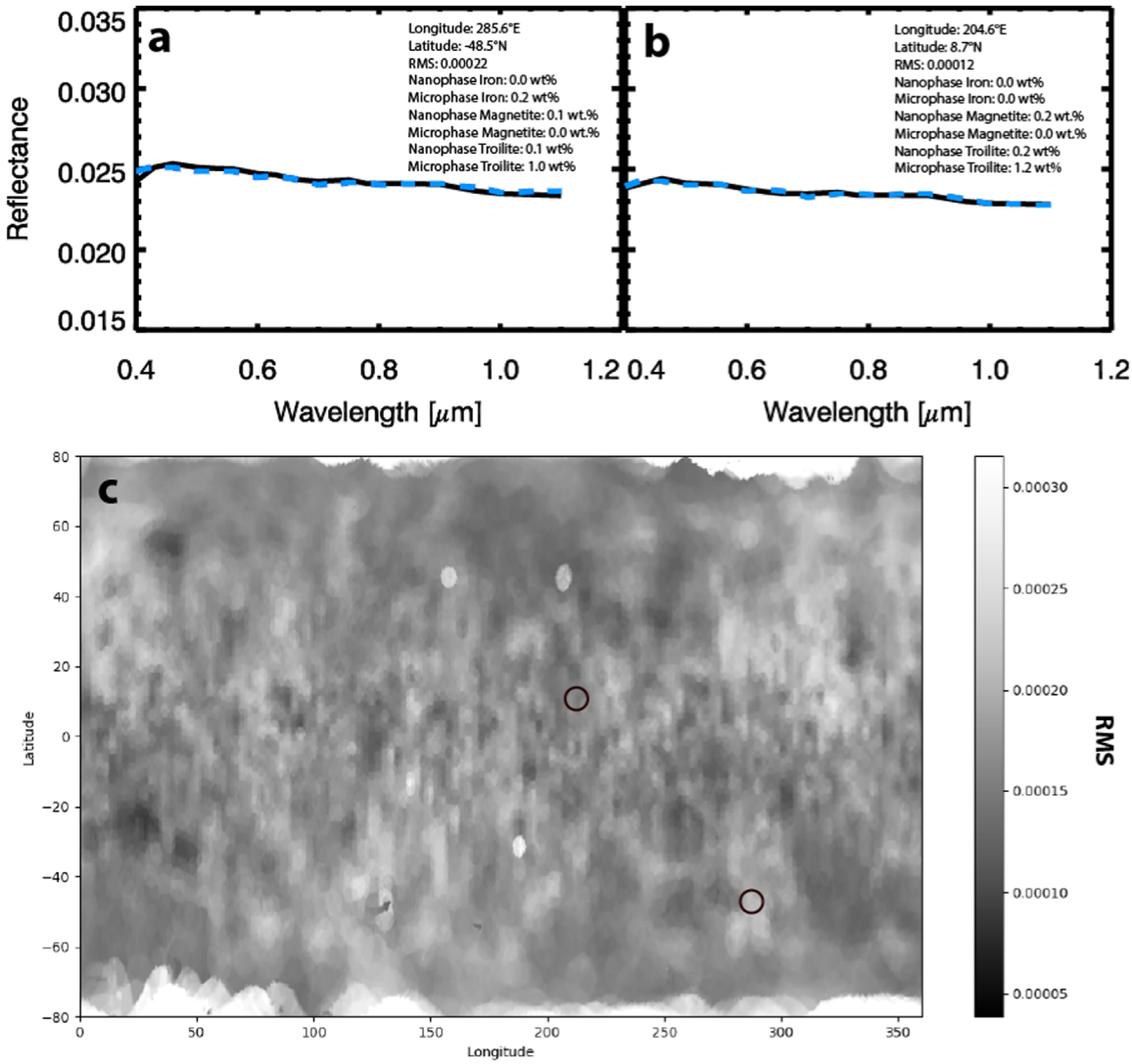

Figure 2. Panels (a) and (b) show examples of two model spectra (blue dashed lines) fitting OVIRS spectra (black solid lines), with their locations shown by the black circles in the rms map in panel (c). These spectra show the quality of fits with an rms of 0.000 22 (a), which makes up most of lighter gray areas on the rms map (c), and an rms of 0.000 12 (b), representing one of the darker gray areas. The rms map shows all areas that were modeled. The poor fits in the polar regions are as expected due to poorer lighting conditions, which are also why Figure 2 only ranges between ±60° latitude.

Because Bennu's surface has a wide range of albedos (Lauretta et al. 2019; DellaGiustina et al. 2020), the greater microphase iron abundances may be due to a few of the darker regions on Bennu's surface (Section 4.4.). Specifically, the model may be artificially compensating for the darker boulders by increasing the abundance of microphase iron particles, because microphase iron causes the spectrum to darken nearly uniformly across the visible to near-infrared wavelengths (Figure 4; Section 4.4). This may make comparisons of submicroscopic particle abundances more difficult between the darker regions and the lighter regions of Bennu. Regardless, if there are iron-bearing anhydrous silicates on the surface of Bennu (e.g., olivine and pyroxene), then there are likely to be submicroscopic iron particles present, as observed in the laboratory (Sasaki et al. 2001; Moroz et al. 2004a; Thompson et al. 2019) and on the S-type asteroid Itokawa (Noguchi et al. 2011).

The abundance maps indicate that magnetite on Bennu's surface is mostly nanophase, not microphase (Figure 3). This is in agreement with space weathering experiments on the CM Murchison meteorite, which found nanophase magnetite within vapor deposits and no microphase magnetite in the melt deposits (Keller & Clemett 2001; Thompson et al. 2019). Magnetite has been directly detected on Bennu (Hamilton et al. 2019; Lauretta et al. 2019).

Nanophase and microphase troilite particles appear to be present across Bennu's surface in relatively high abundances (Figure 3). The presence of both nanophase and microphase troilite is in agreement with laboratory findings (i.e., Keller et al. 2015; Gillis-Davis et al. 2017; Thompson et al. 2019), which showed troilite to range greatly in size, including nanometer- and micron-scale diameters.

4.2. The Cause of Spectral Bluing on Carbonaceous Asteroids

From our modeling, space weathering products that could cause the bluing on carbonaceous asteroids such as Bennu include nanophase and microphase magnetite, and to some extent, microphase troilite. We explore the role of each of these particles in carbonaceous meteorites and their effects on visible to near-infrared reflectance.

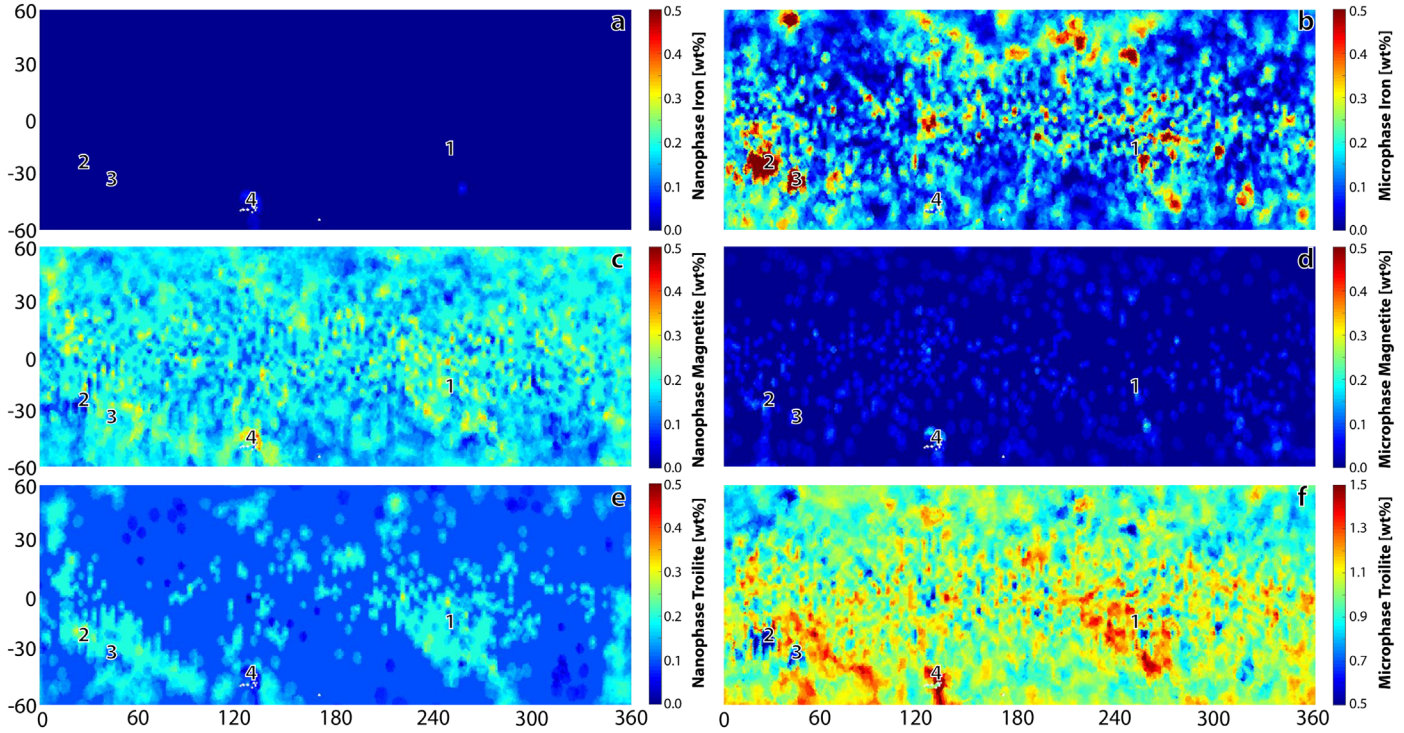

Figure 3. Maps of the modeled abundance of six submicroscopic space weathering products on the surface of asteroid Bennu: (a) nanophase iron, (b) microphase iron, (c) nanophase magnetite, (d) microphase magnetite, (e) nanophase troilite, and (f) microphase troilite. Numbers indicate the region: (1) Tlanuwa Regio, (2) Roc, (3) Huginn, and (4) Benben.

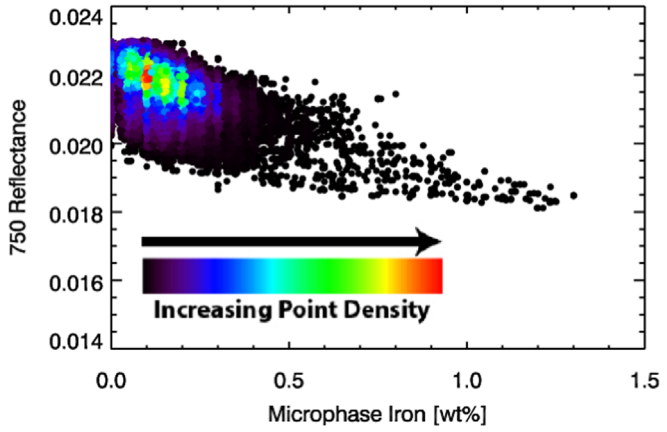

Figure 4. Point density plots showing that, with increasing microphase iron, 750 nm reflectance decreases.

Based upon laboratory work, microphase magnetite is an unlikely culprit for the spectral bluing, because it has not been observed in space weathering experiments and it occurs in negligible modeled abundance across Bennu's surface (Figure 3; Table 4). In contrast, microphase troilite is a product frequently found in space weathering experiments regardless of meteorite type (Keller et al. 2015; Gillis-Davis et al. 2017; Thompson et al. 2019, 2020). However, this space weathering product was found both in meteorites that became spectrally redder and those that became bluer after simulated space weathering (Table 5). Therefore, it is difficult to determine whether microphase troilite plays a deciding role in whether an asteroid becomes redder or bluer with exposure to space weathering.

Solar wind experiments have indicated that carbonization of indigenous organics could also be a cause of bluing (e.g., Moroz et al. 2004b; Lantz et al. 2017). The process of carbonization is likely occurring on Bennu (Simon et al. 2020), which could suggest that solar wind irradiation (e.g., Moroz et al. 2004b; Lantz et al. 2017) is one of the causes of the spectral bluing of carbonaceous asteroids. In studies of carbonaceous meteorites, Lantz et al. (2017) pointed out that, with dehydration, the presence of organics also decreased. Furthermore, some hydrated meteorites, such as CMs, CIs, and Tagish Lake, became bluer in solar wind experiments (Table 1), supporting the notion that carbonization of organics may cause some spectral bluing. However, two of the solar wind experiments on the hydrated meteorite (CM Murchison) found that the visible to near-infrared spectra did not change or became redder (Table 1; Keller et al. 2015; Lantz et al. 2015), which implies that the spectral change is weak. This indicates that carbonization can cause some spectral bluing of asteroids, but is not likely to dictate whether an asteroid will become spectrally bluer or redder. Experiments using ion irradiation will be needed in order to fully grasp the role that carbonization plays on asteroid surfaces.

The remaining candidate for the cause of spectral bluing on carbonaceous asteroids is nanophase magnetite, which shows a moderate abundance across Bennu's surface and has been shown to form in a space weathering experiment (Thompson et al. 2019). Thompson et al. (2019) inferred that nanophase magnetite forms when a micrometeoroid impact is incident upon phyllosilicates (where all minerals in this group have either OH or H_2O) and produces a vapor cloud that contains Fe, S, and OH. Within the vapor cloud, the OH reacts with the Fe and forms magnetite rather than metallic iron. From lunar soils, we know that submicroscopic particles in vapor deposits are smaller in size (i.e., nanophase) than those observed in melt (i.e., microphase) (Keller & Clemett 2001). Because nanophase

Table 5
Summary of Nanophase and Microphase Compositions from Laboratory Experiments and Spectral Modeling of Bennu

Perspective	npFe	mpFe	npMag	mpMag	npTro	mpTro
Spectral Slope	Red	Neutral	Blue	Blue	Red	Blue
Laboratory: Hydrous Meteorites	X	[X]	X		X	X
Laboratory: Anhydrous Meteorites	X	X			X	
Space Weathering Model of Bennu		X	X		X	X

Note. [X] We assume that this could form under actual space weathering conditions as seen from lunar samples.
References. (1) Keller et al. 2015; (2) Matsuoka et al. 2015; (3) Gillis-Davis et al. 2017; (4) Thompson et al. 2020.

magnetite was only observed in the vapor deposit and its presence did not withstand continued simulated space weathering, it is unlikely that the micrometeoroid impacts on Bennu's surface would produce microphase magnetite. Although the bombardment of solar wind particles on the surfaces of an asteroid is also an important component of space weathering, it is not known whether this process could efficiently produce nanophase magnetite.

The importance of phyllosilicates in producing spectral bluing is supported by other space weathering experiments. In experiments that simulated micrometeoroid bombardment on meteorites, the samples that became darker and bluer (CMs, CIs, Tagish Lake) contained hydrated minerals (Hiroi et al. 2013; Matsuoka et al. 2015, 2020; Thompson et al. 2019, 2020) (see Table 1). One experiment that simulated micrometeoroid bombardment on a hydrous carbonaceous chondrite (CM2 Mighei) led to spectral reddening, but the experiment occurred over material that was dominated by olivine (i.e., OH was not available to oxidize the Fe) (Moroz et al. 2004a), and space-weathered olivine forms nanophase iron. Additionally, terrestrial Fe-dominated phyllosilicates subjected to micrometeoroid bombardment experiments initially became redder, but then became bluer with longer exposures to space weathering (Kaluna et al. 2017). Thus, we infer that hydrated minerals are needed for space-weathered surfaces of asteroids to become bluer.

Micrometeoroid bombardment experiments on anhydrous carbonaceous meteorites (CV, CO, and CK types) led to spectral reddening (Hiroi et al. 2013; Gillis-Davis et al. 2017) (see Table 1), which further supports our interpretation. Specifically, the micrometeoroid impacts formed nanophase iron and sulfides (e.g., troilite and pentlandite). These experiments did not produce any magnetite, which we suggest is due to the lack of OH available in the samples to oxidize the iron particles (Table 3).

Another important component may be availability of FeO. Micrometeoroid bombardment experiments on terrestrial Mg-dominated phyllosilicates showed slight reddening (Kaluna et al. 2017). Although the experiment occurred on a hydrated mineral, we infer that the lack of FeO in the mineral did not allow the sample to form magnetite—and therefore it could not become spectrally bluer. The amount of FeO needed on the surface to produce magnetite may be as little as a few weight percent, based upon observations of lunar space weathering producing metallic iron (Trang & Lucey 2019), which is consistent with the presence of Mg/Fe phyllosilicates as observed on Bennu (Hamilton et al. 2019; Simon et al. 2020).

OH/H_2O produces a distinct $\sim$3 μm absorption feature in the near-infrared, which is commonly used to detect their presence of hydrated phyllosilicates. Based on our inference that OH/H_2O are required to produce nanophase magnetite and spectral bluing, we predict that asteroids with a strong 3 μm feature are bluer (assuming the presence of Fe in the phyllosilicates). Likewise, we predict that asteroids with weak 3 μm absorption features are redder. Near-infrared reflectance spectra returned from OSIRIS-REx show that Bennu exhibits a strong 3 μm absorption and is also spectrally blue in the visible to near-infrared (Hamilton et al. 2019). In contrast, Hayabusa2's observation of Ryugu showed that it is spectrally red and displays a weak 3 μm absorption (Kitazato et al. 2019). This weak 3 μm absorption may be due to Ryugu either having a low abundance of OH since its formation or having been dehydrated after formation (Sugita et al. 2019). If Ryugu has been dehydrated, then earlier in its (more hydrated) history, space weathering would have produced nanophase magnetite. After dehydration of Ryugu, continued space weathering on the surface would either reprocess these nanophase magnetite particles and convert them to nanophase iron or cover them with metallic iron, which would create nanophase particles with a magnetite core and a metallic iron rim. Such layered nanophase particles would be similar to those observed in lunar samples (e.g., Thompson et al. 2016). These spectral observations of asteroids support the role of phyllosilicate precursors in spectral bluing. Because samples are being returned from Ryugu and Bennu, we have the opportunity to test predictions: We predict that samples of Bennu will exhibit nanophase and microphase iron and sulfides and nanophase magnetite with relatively higher abundances of magnetite than iron. In contrast, samples of Ryugu will have nanophase and microphase iron and sulfides, but will lack (or have very low abundances of) nanophase magnetite. Examining the composition of the nanophase iron particles from core to the rim could potentially shed light on Ryugu's geologic history, as the core may be more representative of Ryugu's earlier geologic history and the rim of these particles could be representative of more present day. Thus, if the core contains more magnetite and the rim contains more iron, this would suggest that Ryugu did dehydrate over its lifetime.

4.3. Comparison between Modeled Submicroscopic Particle Abundances

We examined the relationship between the abundances of the six modeled submicroscopic particles (Figure 3) in order to understand the reasonableness of the model results. Because space weathering produces nanophase particles first (e.g., Pieters & Noble 2016), we compared the modeled nanophase particle abundances against other submicroscopic particle abundances. The modeled nanophase magnetite abundance appears to be positively correlated with other space weathering products, including nanophase iron and nanophase troilite, but with considerable scatter (see panels (a) and (b) of Figure 5). Although for most of Bennu's surface, nanophase iron

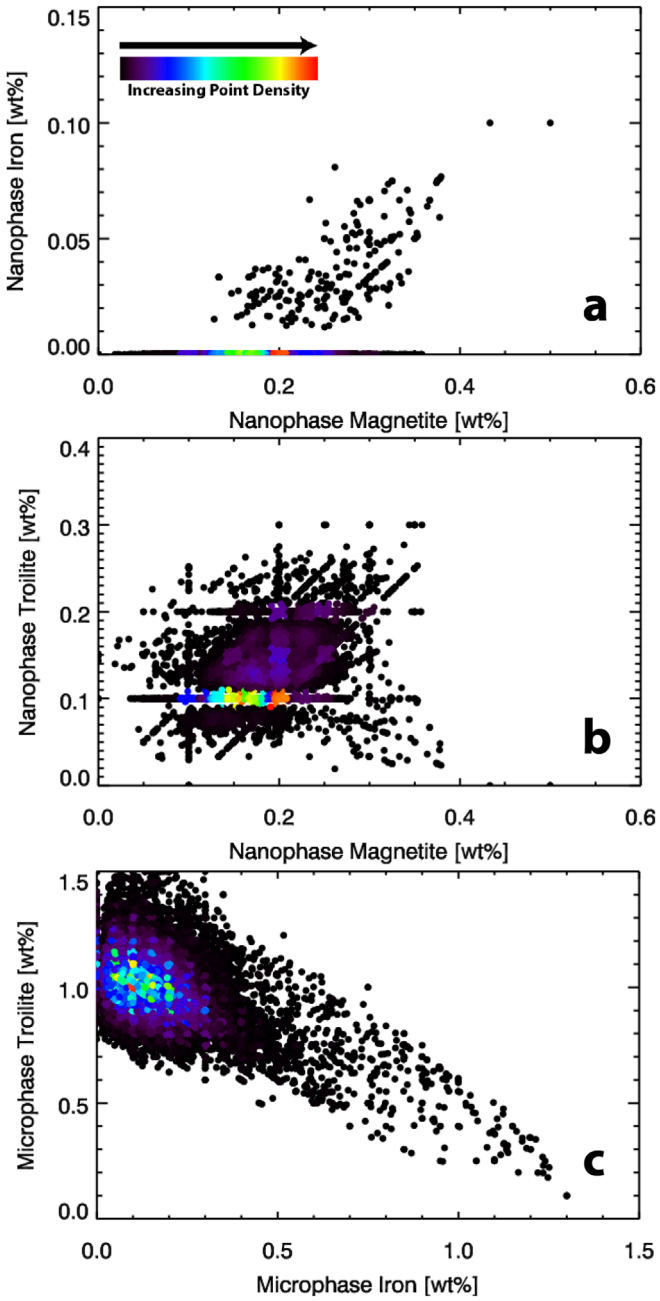

Figure 5. (a) Density plot of nanophase magnetite and nanophase iron abundances, illustrating that in areas containing nanophase iron, there is an increase in nanophase iron abundance relative to nanophase magnetite abundance. (b) Density plot of nanophase magnetite abundance with respect to nanophase troilite abundance, which shows a loose positive correlation between the two particle types. The horizontal and vertical clusters of points (e.g., 0.1 and 0.2 wt% troilite and 0.1 and 0.2 wt% magnetite) are due to the averaging of points. (c) Density plot of microphase iron and microphase troilite abundances, showing an apparent inverse relationship, which may indicate the proportion of sulfides to silicates in a region.

abundance is 0.0 wt%, in areas that contain nanophase iron, the nanophase magnetite is = 0.2 wt% (Figure 5(a)). We infer that this is because the high abundance of phyllosilicates allows a better chance of producing nanophase magnetite than metallic Fe. We predict that, after a certain threshold (as these abundances are relative abundance and not absolute) of nanophase magnetite is present on the surface, nanophase iron begins to form, because after long exposures to space weathering, the hydrated minerals become less accessible to the space weathering process. We conclude that this is because these minerals are gradually covered underneath a patina of anhydrous glass and therefore OH is not readily available. Concurrently, the microstructural decomposition of phyllosilicates, evidenced by laboratory experiments (e.g., Thompson et al. 2019, 2020), results in the loss and degassing of structural OH with continued exposure to space weathering. The loss of OH and the reduction in its availability promotes the formation of nanophase metallic iron under these newly reducing conditions. Meanwhile, modeled nanophase troilite roughly correlates in abundance with nanophase magnetite. This relationship suggests that nanophase troilite forms concurrently and is not dependent on the availability of OH, only on the availability of S, as expected from laboratory experiments (e.g., Matsuoka et al. 2015; Thompson et al. 2020) (see Figure 5(b)).

From a space weathering perspective, the relatively high abundances of modeled microphase troilite was unexpected (Figure 5(c)). This model result could indicate that (1) production of microphase troilite via space weathering is fast relative to that of other submicroscopic particles, (2) Bennu's surface materials started with a high microphase troilite abundance, or (3) our assumed model host reflectance favored anomalously more microphase troilite (explored further in Section 4.4). The second conclusion is supported by analyses of CM chondrites that have found indigenous sulfides (e.g., Bullock et al. 2010). These observations indicate that there may have been micron-sized troilite already present in the materials that now make up the surface of Bennu, even before they were exposed to space weathering.

On the other hand, assuming that the modeled microphase iron abundance is not artificially compensating for the darker boulders on Bennu (see Sections 4.1 and 4.4), the faster production of microphase troilite through space weathering could explain the inverse relationship between the modeled microphase iron and troilite abundances (Figure 5(c)). Assuming that the modeled microphase troilite and iron originate through space weathering, this inverse relationship may indicate the proportion of silicates to sulfides on the surface. Thus, regions lacking sulfides as a source for S would produce only microphase iron, whereas regions rich in sulfides would instead produce microphase troilite. Regions containing some mixed abundances of sulfides and silicates would be between the two endmembers. If this is the case, we infer that the presence and proportion of sulfides to silicates controls the ratio of microphase troilite to iron, which appears to be in agreement with space weathering experiments (Keller et al. 2013). An alternative explanation to this inverse relationship may be that space weathering on Bennu's surface dominantly produces submicroscopic sulfides, which may in turn decompose into submicroscopic iron with further exposure. Evidence of troilite grains decomposing to iron has been observed in Itokawa samples (Matsumoto et al. 2020). The returned samples from OSIRIS-REx will show which (if not both (1) and (2)) of these interpretations explain(s) the high abundance of microphase troilite.

4.4. Changes in Modeling Assumptions

In our model, we made several assumptions that do not fully capture the complexity of Bennu's surface characteristics. Specifically, Bennu's surface consists mostly of boulders with different physical and spectral properties

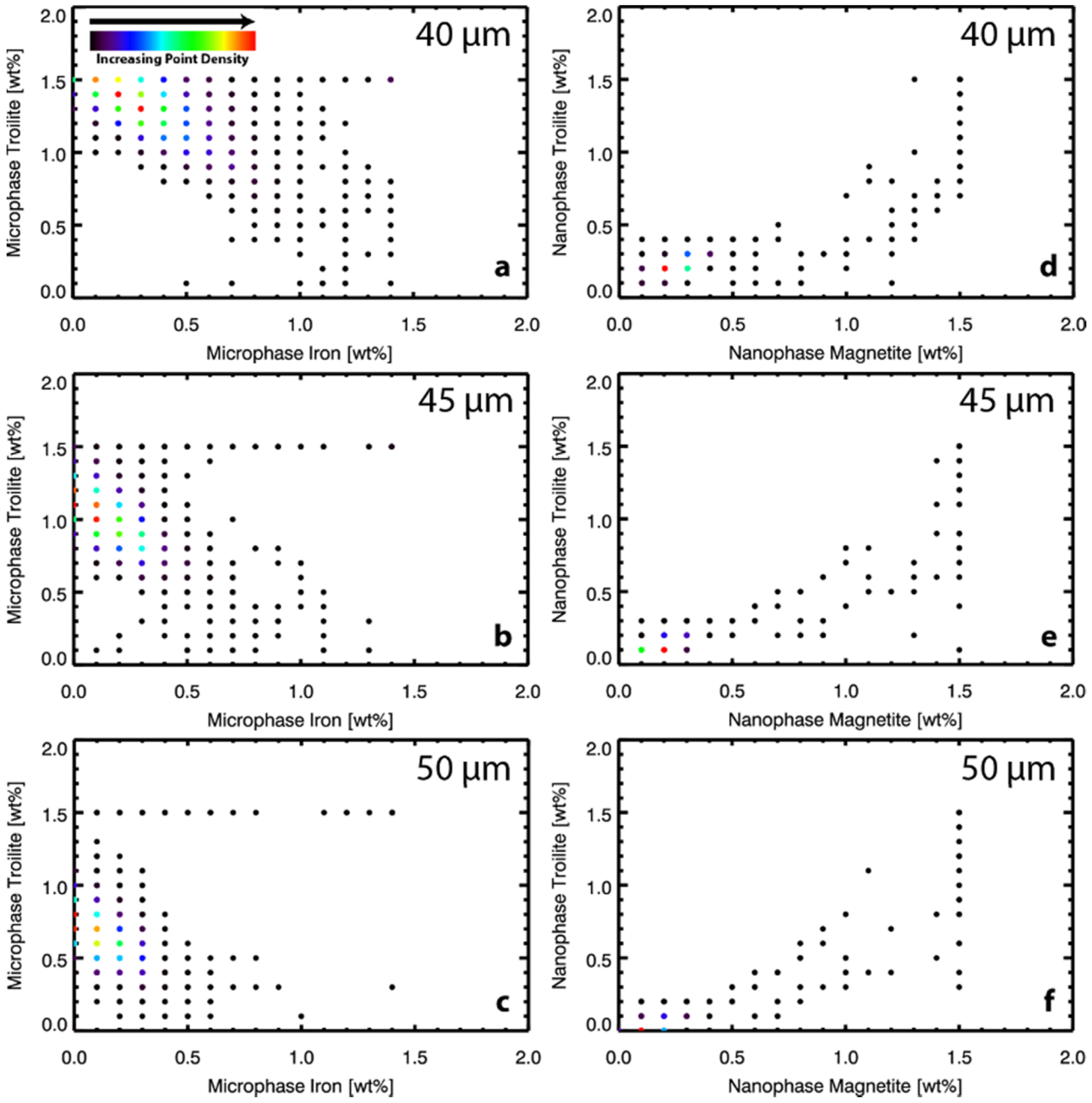

Figure 6. Point density plots comparing microphase iron and microphase troilite (left column) and nanophase magnetite and nanophase troilite (right column). Top, middle, and bottom rows correspond to models run with particle sizes of 40, 45, and 50 μm, respectively. The relative proportions of microphase iron and troilite are preserved. The relationship between nanophase magnetite and nanophase troilite shows that nanophase magnetite abundances does not change much with the size of the host particles, whereas nanophase troilite abundance changes with host particle size.

(DellaGiustina et al. 2019, 2020). Although our model assumes that the surface of Bennu consists of powdered regolith of uniform composition—which is not completely the case (e.g., Hamilton et al. 2021, in revision)—we assume that the particle size in our model is likely capturing the surface roughness of these boulders. Because the radiative transfer model is sensitive to the cross-sectional area of particles (Hapke 2001), we assumed that the surface roughness of boulders acts similarly to a particulate medium (which also contains cavities between particles), but the grains are glued together. We tested how the model results respond to changes in the particle size parameter. Although our changes are by several microns, changes in tens of microns could result in changes by several percent in overall reflectance. At 40 and 50 μm, the proportions between the microphase iron and troilite remain the same (Figure 6(a)–(c)). For the modeled nanophase magnetite and nanophase troilite abundances, the nanophase magnetite abundance appears similar to abundances modeled using a grain size of 45 μm, and the nanophase troilite shows very minor changes (Figure 6(d)–(f)). Therefore, nanophase magnetite abundance appears insensitive to particle size or surface roughness, giving us confidence in the modeled abundances. The microphase iron and troilite abundances appear to be consistent as long as their relative abundances are compared to one another rather than to magnetite.

We assumed a host particle with the same optical properties across Bennu's surface; however, images show areas on

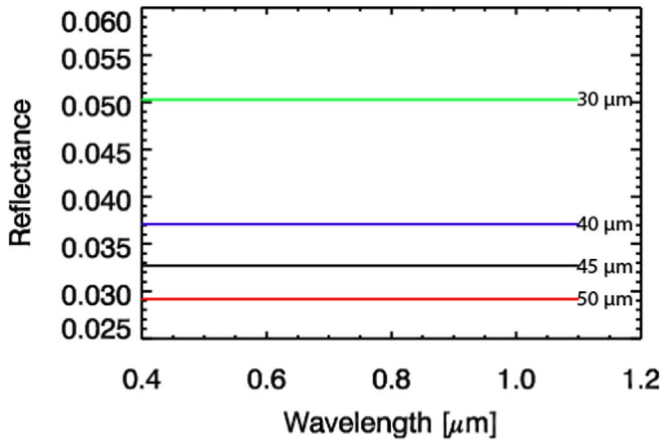

Figure 7. Plot of how changing the host particle size in the radiative transfer model results in consistent change in reflectance in the visible to near-infrared.

Bennu's surface with high and low albedos. Because we used the same host reflectance (i.e., the reflectance without any submicroscopic particle or reflectance of the unweathered surface) for each OVIRS spectrum (assuming the same composition across Bennu's surface), surfaces that have lower albedo, because it consists of darker minerals, will likely have higher modeled abundances of submicroscopic particles, as more submicroscopic particles are needed in the regolith to lower the model reflectance to match the OVIRS spectrum of these dark areas (Figure 2). We also tested what happens when the host reflectance is uniformly increased and decreased (still a constant across all visible to near-infrared wavelengths). The effects are similar to those of changing the particle size (e.g., Trang et al. 2013) (see Figure 7). Thus, we suggest that the low and high relative abundances of nanophase magnetite are also insensitive to host reflectance, and the iron and troilite abundances should be the same relative to one another.

One of our assumptions is that the host reflectance does not contain any spectral features (e.g., spectral absorptions and peaks), which could affect the quality of fit between our model reflectance spectra and the OVIRS spectra. Based upon space weathering studies of the Moon, small spectral features are unlikely to affect the quality of fit because one of the main spectral effects of space weathering on lunar soil is weakening absorption features (e.g., Hapke 2001). Thus, any small spectral features that are a result of the host material are likely to weaken with increasing submicroscopic particle abundance.

Another assumption is that the host reflectance is constant instead of having a sloped visible to near-infrared spectrum. We can speculate how it would affect the overall model submicroscopic particle abundances. For example, a red-sloped host reflectance would require more submicroscopic particles that would make the model spectrum "bluer" to match the OVIRS spectrum and fewer particles that make the model spectrum "redder" relative to model abundances based upon a constant host reflectance. This would suggest that the model spectrum would likely include more modeled nanophase magnetite and potentially microphase troilite and microphase magnetite, and less modeled nanophase iron and nanophase troilite. Conversely, a host reflectance that starts off "bluer" than a constant host reflectance would suggest lower abundances of nanophase magnetite and higher abundances of nanophase iron and troilite, to make the model spectrum "redder" and thus match the OVIRS spectrum. This relationship between host reflectance slope and submicroscopic particle abundance is a potential explanation for the high microphase troilite abundance observed in our maps (Figure 2(f)). Because Bennu is similar to CM/CI chondrites (Clark et al. 2011; Hamilton et al. 2019), these meteorites would make an ideal starting composition. However, using these compositions with our model presents several issues. First, the overall reflectance and shape of a visible and near-infrared spectrum of a CM meteorite is dependent on particle size and density (e.g., Cloutis et al. 2011), and without samples from Bennu, we do not know which reflectance best represents the surface. Another issue is that carbonaceous meteorites contain opaques, which would complicate our model because our model works only with transparent minerals (e.g., Trang & Lucey 2019) and we do not have a method to compensate for the varying opaque abundances on Bennu's surface. Also, the average indices of refraction (n and k) CM and CI are not easily determined, due to the fact that the materials consist of mineral mixtures, which are required quantities for producing a model host particle.

5. Conclusions

We used a Hapke radiative transfer model to investigate why some carbonaceous asteroids become spectrally bluer instead of spectrally redder with exposure to space weathering. By modeling spectral data from the OSIRIS-REx mission of the hydrated, spectrally blue carbonaceous asteroid Bennu, and comparing our model results with laboratory-based space weathering experiments, we infer that nanophase magnetite is the most likely cause of spectral bluing. We reason that, for a carbonaceous asteroid to become spectrally bluer, hydrated iron-bearing phyllosilicates, which enable the formation of nanophase magnetite, need to be present on the surface. Without these hydrated minerals or the availability of H_2O or OH, we posit that space weathering preferentially forms nanophase iron, which causes spectral reddening. From this conclusion, we can predict that the samples returned from Ryugu by Hayabusa2 will contain submicroscopic iron and sulfides (i.e., troilite) because Ryugu is dehydrated and spectrally red, whereas samples returned from Bennu by OSIRIS-REx will contain submicroscopic iron, magnetite, and sulfides, with nanophase magnetite having a greater relative abundance than iron.

We further infer that, after some amount of nanophase magnetite particles are produced on Bennu's surface, nanophase iron particles begin to form, which may be related to the decreased availability of H_2O or OH on the grain surface that has been used to form nanophase magnetite or lost from the system. Our model results suggest that the surface of Bennu contains a high abundance of microphase troilite. This could be explained by the fact that micron-sized troilite is indigenous to Bennu and is not a product of space weathering. On the other hand, if the varying modeled microphase iron abundance is not an artifact that is compensating for the darker albedo of boulders on Bennu, and space weathering produces troilite at an accelerated rate relative to other submicroscopic particles, then this observation could explain the inverse relationship between microphase troilite and microphase iron. This would suggest that the availability of S in a system controls whether space weathering will form more microphase troilite or more microphase iron.

This work is supported by NASA under contract NNM10AA11C issued through the New Frontiers Program and the NASA OSIRIS-Rex Participating Scientist Program 80NSC18K0230 to D.T. We are grateful to the entire OSIRIS-REx team for making the encounter with Bennu possible. We would also like to thank the two anonymous reviewers for their professionally written, constructive, and helpful comments, as well as Cat Wolner for polishing the manuscript, and the amazing Jemma Davidson for helping us find key references. SOEST publication #11282. HIGP #2441.

ORCID iDs

David Trang https://orcid.org/0000-0002-2924-7555
Beth E. Clark https://orcid.org/0000-0002-2407-2880
Jian-Yang Li https://orcid.org/0000-0003-3841-9977
Amy A. Simon https://orcid.org/0000-0003-4641-6186
Daniella N. DellaGiustina https://orcid.org/0000-0002-5643-1956
Kevin J. Walsh https://orcid.org/0000-0002-0906-1761
Dante S. Lauretta https://orcid.org/0000-0002-2597-5950

References

Barnouin, O. S., Daly, M. G., Palmer, E. E., et al. 2020, P&SS, 180, 104764
Bennett, C. A., DellaGiustina, D. N., Becker, K. J., et al. 2020, Icar, 357, 113690
Brunetto, R., Lantz, C., Ledu, D., et al. 2014, Icar, 237, 278
Bullock, E., McKeegan, K. D., Gounelle, M., Grady, M. M., & Russell, S. S. 2010, M&PS, 45, 885
Cahill, J. T. S., Blewett, D. T., Nguyen, N. V., et al. 2012, GeoRL, 39, L10204
Cassidy, W., & Hapke, B. 1975, Icar, 25, 371
Clark, B. E., Binzel, R. P., Howell, E. S., et al. 2011, Icar, 216, 462
Cloutis, E. A., Hudon, P., Hiroi, T., Gaffey, M. J., & Mann, P. 2011, Icar, 216, 309
DellaGiustina, D. N., Burke, K. N., Walsh, K. J., et al. 2020, Sci, 370, eabc3660
DellaGiustina, D. N., Emery, J. P., Golish, D. R., et al. 2019, NatAs, 3, 341
Egan, W. G., & Hilgeman, T. 1977, Icar, 30, 413
Gao, L., Lemarchand, F., & Lequime, M. 2012, OExpr, 20, 15734
Gillis-Davis, J. J., Lucey, P. G., Bradley, J. P., et al. 2017, Icar, 286, 1
Hamilton, V. E., Christensen, P. R., Kaplan, H. H., et al. 2021, A&A, submitted
Hamilton, V. E., Simon, A. A., Christensen, P. R., et al. 2019, NatAs, 3, 332
Hapke, B. 2001, JGR, 106, 10039
Hapke, B. 2012, Icar, 221, 1079
Hiroi, T., Milliken, R. E., Robertson, K. M., et al. 2020, LPSC, 51, 1043
Hiroi, T., Sasaki, S., Misu, T., & Nakamura, T. 2013, LPSC, 44, 1276
Kaluna, H. M., Ishii, H. A., Bradley, J. P., Gillis-Davis, J. J., & Lucey, P. G. 2017, Icar, 292, 245
Keller, L. P., & Clemett, S. J. 2001, LPSC, 32, 2097
Keller, L. P., & McKay, D. S. 1993, Sci, 261, 1305
Keller, L. P., Christoffersen, R., Dukes, C. A., Baragiola, R., & Rahman, Z. 2015, LPSC, 46, 1913
Keller, L. P., & McKay, D. S. 1997, GeCoA, 61, 2331
Keller, L. P., Rahman, Z., Hiroi, T., et al. 2013, LPSC, 44, 2404
Kitazato, K., Milliken, R. E., Iwata, T., et al. 2019, Sci, 364, 272
Krot, A. N., Keil, K., Scott, E. R. D., Goodrich, C. A., & Weisberg, M. K. 2014, Meteorites and Cosmochemical Processes, Vol. 1 of Treatise on Geochemistry (2nd ed.; Amsterdam: Elsevier), 1
Laczniak, D. L., Thompson, M. S., Dukes, C. A., et al. 2020, LPSC, 51, 2667
Lantz, C., Brunetto, R., Barucci, M. A., et al. 2015, A&A, 577, A41
Lantz, C., Brunetto, R., Barucci, M. A., et al. 2017, Icar, 285, 43
Lauretta, D. S., Balram-Knutson, S. S., Beshore, E., et al. 2017, SSRv, 212, 925
Lauretta, D. S., Dellagiustina, D. N., Bennett, C. A., et al. 2019, Natur, 568, 55
Lauretta, D. S., Enos, H. L., Polit, A. T., et al. 2021, in Sample Return Missions, ed. A. Longobardo (Amsterdam: Elsevier) in press
Lazzarin, M., Marchi, S., Moroz, L. V., et al. 2006, ApJL, 647, L179
Lucey, P. G. 1998, JGR, 103, 1703
Lucey, P. G., & Riner, M. A. 2011, Icar, 212, 451
Matsumoto, T., Harries, D., Langenhorst, F., Miyake, A., & Noguchi, T. 2020, NatCo, 11, 1117
Matsuoka, M., Nakamura, T., Hiroi, T., Okumura, S., & Sasaki, S. 2020, ApJL, 890, L23
Matsuoka, M., Nakamura, T., Kimura, Y., et al. 2015, Icar, 254, 135
Moroz, L., Baratta, G., Strazulla, G., et al. 2004b, Icar, 170, 214
Moroz, L. V., Shingareva, T. V., Basilevsky, A. T., et al. 2004a, LPSC, 35, 1279
Mustard, J. F., & Pieters, C. M. 1989, JGR, 94, 13619
Nesvorný, D., Jedicke, R., Whiteley, R. J., & Ivezić, Ž. 2005, Icar, 173, 132
Noble, S. K., Pieters, C. M., & Lindsay, P. 2007, Icar, 192, 629
Noguchi, T., Kimura, M., Hashimoto, T., et al. 2014, M&PS, 49, 188
Noguchi, T., Nakamura, T., Kimura, M., et al. 2011, Sci, 333, 1121
Pieters, C. M., & Noble, S. K. 2016, JGRE, 121, 1865
Querry, M. R. 1985, Optical Constants (Kansas City, MO: Missouri Univ.)
Reuter, D. C., Simon, A. A., Hair, J., et al. 2018, SSRv, 214, 54
Reuter, D. C., Simon, A. A., Lunsford, A., et al. 2019, Origins, Spectral Interpretation, Resource Identification, Security, Regolith Explorer (OSIRIS-REx): Visible and InfraRed Spectrometer (OVIRS) Bundle. NASA Planetary Data System, https://sbn.psi.edu/pds/resource/orex/ovirs.html
Rubino, S., Lantz, C., Baklouti, D., et al. 2020, PSJ, 1, 61
Sasaki, S., Nakamura, K., Hamabe, Y., Kurahashi, E., & Hiroi, T. 2001, Natur, 410, 555
Scott, E. R. D., & Krot, A. N. 2007, TrGeo, 1, 1
Simon, A. A., Kaplan, H. H., Hamilton, V. E., et al. 2020, Sci, 370, eabc3522
Sugita, S., Honda, R., Morota, T., et al. 2019, Sci, 364, 252
Thompson, M., Morris, R. V., Clemett, S. J., et al. 2020, Icar, 346, 113775
Thompson, M. S., Loeffler, M. J., Morris, R. V., Keller, L. P., & Christoffersen, R. 2019, Icar, 319, 499
Thompson, M. S., Zega, T. J., Becerra, P., Keane, J. T., & Byrne, S. 2016, M&PS, 51, 1082
Trang, D., & Lucey, P. G. 2019, Icar, 321, 307
Trang, D., Lucey, P. G., Gillis-Davis, J. J., et al. 2013, JGRE, 118, 708
Trang, D., Lucey, P. G., & Izenberg, N. R. 2017, Icar, 293, 206
Vernazza, P., Fulvio, D., Brunetto, R., et al. 2013, Icar, 225, 517
Zou, X.-D., Li, J.-Y., Clark, B. E., et al. 2021, Icar, 358, 114183